

N 73-19999

NASA TECHNICAL NOTE



NASA TN D-7251

NASA TN D-7251

CASE FILE
COPY

STEADY, SUBSONIC, LIFTING
SURFACE THEORY FOR WINGS
WITH SWEEP, PARTIAL SPAN,
TRAILING EDGE CONTROL SURFACES

by Richard T. Medan

Ames Research Center

Moffett Field, Calif. 94035

1. Report No. NASA TN D-7251		2. Government Accession No.		3. Recipient's Catalog No.	
4. Title and Subtitle STEADY, SUBSONIC, LIFTING SURFACE THEORY FOR WINGS WITH SWEEP, PARTIAL SPAN, TRAILING EDGE CONTROL SURFACES				5. Report Date April 1973	
				6. Performing Organization Code	
7. Author(s) Richard T. Medan				8. Performing Organization Report No. A-4521	
				10. Work Unit No. 760-74-01-07	
9. Performing Organization Name and Address NASA Ames Research Center Moffett Field, Calif., 94035				11. Contract or Grant No.	
				13. Type of Report and Period Covered Technical Note	
12. Sponsoring Agency Name and Address National Aeronautics and Space Administration Washington, D. C. 20546				14. Sponsoring Agency Code	
15. Supplementary Notes					
16. Abstract <p>A method for computing the lifting pressure distribution on a wing with partial span, swept control surfaces is presented. This method is valid within the framework of linearized, steady, potential flow theory and consists of using conventional lifting surface theory in conjunction with a flap pressure mode. The cause of a numerical instability that can occur during the quadrature of the flap pressure mode is discussed, and an efficient technique to eliminate the instability is derived. This technique is valid for both the flap pressure mode and regular pressure modes and could be used to improve existing lifting surface methods. Examples of the use of the flap pressure mode and comparisons among this method, other theoretical methods, and experiments are given. Discrepancies with experiment are indicated and candidate causes are presented. It is concluded that the method can lead to an efficient and accurate solution of the mathematical problem when a partial span, trailing edge flap is involved.</p>					
17. Key Words (Suggested by Author(s)) Potential flow Three-dimensional flow Inviscid flow Kernel functions Wing Flaps Lifting surface Control surface				18. Distribution Statement Unclassified - Unlimited	
19. Security Classif. (of this report) Unclassified		20. Security Classif. (of this page) Unclassified		21. No. of Pages 35	22. Price* \$3.00

NOTATION

b	wing span
$b_j(\eta)$	quadrature coefficient
c	local chord
$C_{H\delta}$	rate of change of hinge moment coefficient with flap deflection angle measured at $\alpha = 0^\circ$
$C_{\ell\delta}$	rate of change of rolling moment coefficient with flap deflection angle measured at $\alpha = 0^\circ$
$C_{L\delta}$	rate of change of lift coefficient with flap deflection angle measured at $\alpha = 0^\circ$
Δc_ℓ	change in section lift coefficient due to flap deflection
ΔC_L	change in overall lift coefficient due to flap deflection
ΔC_p	differential pressure coefficient
$E(m)$	complete elliptic integral of the second kind with parameter m
h	function that need not be precisely defined for the purpose of the section in which it is used
$h_n(\xi)$	chordwise pressure mode
J	number of stations used in performing a numerical integration
$K(m)$	complete elliptic integral of the first kind with parameter m
M	Mach number; also an integer representing the number of integration points used in some particular numerical quadrature
N	number of chordwise control points
$x_c(\eta)$	position of the hinge line or its extension measured relative to the 50-percent chord line and made dimensionless by the local semi-chord; $-1 < x_c < +1$
α	streamwise slope of the wing mean camber surface
β	$\sqrt{1 - M^2}$
δ	difference or an error or a control surface deflection angle
δ_0	constant used to control the overall accuracy of the chordwise integrations

ϵ quantity meant to be a constant or to shrink to zero in some process
 η_1, η_2 spanwise positions of the flap side edges $|\eta_2| \geq |\eta_1|$ and $\eta_2 > 0$
 λ_c sweep angle of the control surface hinge line
 ξ, η, z coordinates made dimensionless by the semispan, see figure 1 (primes are used when the coordinate is an integration variable)
 \sim symbol implying proportionality

Subscripts

c,f control surface or flap
j particular spanwise station
le leading edge
te trailing edge

STEADY, SUBSONIC, LIFTING SURFACE THEORY FOR WINGS WITH
SWEPT, PARTIAL SPAN, TRAILING EDGE CONTROL SURFACES

Richard T. Medan

Ames Research Center

SUMMARY

A method for computing the lifting pressure distribution on a wing with partial span, swept control surfaces is presented. This method is valid within the framework of linearized, steady, potential flow theory and consists of using conventional lifting surface theory in conjunction with a flap pressure mode. The cause of a numerical instability that can occur during the quadrature of the flap pressure mode is discussed and an efficient technique to eliminate the instability is derived. This technique is valid for both the flap pressure mode and regular pressure modes and could be used to improve existing lifting surface methods. Examples of the use of the flap pressure mode and comparisons among this method, other theoretical methods, and experiments are given. Discrepancies with experiment are indicated and candidate causes are presented. It is concluded that the method can lead to an efficient and accurate solution of the mathematical problem when a partial span, trailing edge flap is involved.

INTRODUCTION

Linearized, subsonic lifting surface theory for predicting lifting pressure distributions and the associated loads and moments on wings having arbitrary planform and smooth surface slope distributions has been well developed. This is not the case for wings having surface slope discontinuities, however. Various methods for solving the control surface problem have been devised, but all seem to possess inadequacies that result from not accurately portraying the pressure distribution near the corner and at the side edges of the control surface. Landahl (ref. 1) has determined the form and strength of the singular parts of the pressure distribution. This report will show how his results, suitably modified for a swept flap and specialized to the steady case, were incorporated into an existing lifting surface theory. These results can also be easily incorporated into lifting surface methods based on the theories of Multhopp (ref. 2), Truckenbrodt (ref. 3), and Hsu and Weatherill (ref. 4). Furthermore, the methods used herein indicate how the accuracy and efficiency of existing, conventional lifting surface methods can be improved.

BASIC APPROACH

The fundamental equation of linearized, steady lifting surface theory is

$$\alpha(\xi, \eta) = \frac{-1}{8\pi} \lim_{z \rightarrow 0} \frac{\partial}{\partial z} \int_{-1}^{+1} \int_{\xi_{le}(\eta')}^{\xi_{te}(\eta')} \frac{z \Delta C_p(\xi', \eta')}{(\eta - \eta')^2 + z^2} \bar{K}[\xi - \xi', \beta(\eta - \eta')] d\xi' d\eta' \quad (1)$$

where

$$\bar{K}[\xi - \xi', \beta(\eta - \eta')] = 1 + \frac{\xi - \xi'}{\sqrt{(\xi - \xi')^2 + \beta^2(\eta - \eta')^2 + \beta^2 z^2}} \quad (2)$$

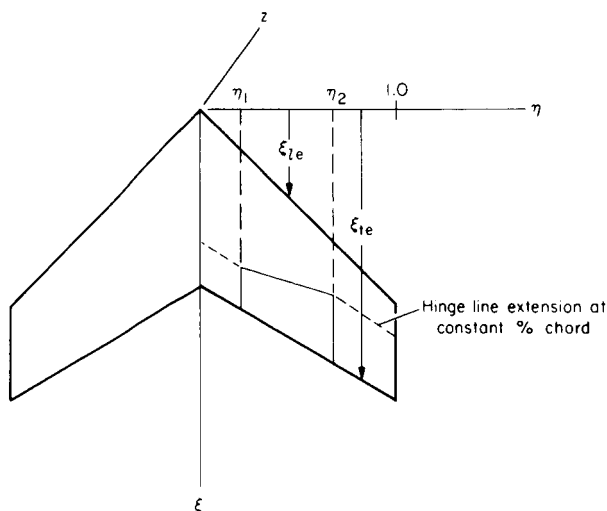


Figure 1.- Definition of coordinate system.

(see fig. 1). This equation is the mathematical expression of the fact that the wing is represented by a distribution of semiinfinite line doublets with strengths proportional to ΔC_p and with their end points placed on the wing and at downstream infinity (see ref. 5 for a derivation). In the analysis problem, $\alpha(\xi, \eta)$ is given and $\Delta C_p(\xi', \eta')$ must be determined. The limit and differentiation processes can be interchanged with the integration if special procedures are observed when the integrations are performed. Thus the integral equation is usually written as

$$\alpha(\xi, \eta) = \frac{-1}{8\pi} \int_{-1}^{+1} \int_{\xi_{le}(\eta')}^{\xi_{te}(\eta')} \frac{\Delta C_p(\xi', \eta')}{(\eta - \eta')^2} \bar{K}[\xi - \xi', \beta(\eta - \eta')] d\xi' d\eta' \quad (3)$$

(The cross on the integral sign symbolically designates these procedures.)

The method for solving this integral equation for a wing of arbitrary planform is to first express the unknown $\Delta C_p(\xi', \eta')$ in terms of known functions with unknown coefficients. The functions generally used are obtained from a consideration of two-dimensional airfoil and lifting line theories. A convenient expansion, based on the theories of Multhopp and Truckenbrodt, is that used by Wagner (ref. 6):

$$\Delta C_p(\xi', \eta') = \frac{2b}{c(\eta)} \sum_{n=1}^N h_n(\xi') f_n(\eta') \quad (4)$$

The prescribed functions h_n are taken from two-dimensional airfoil theory and are comprised of the familiar $\cot \phi/2, \sin \phi, \sin 2\phi, \dots$, terms. The f_n terms are still unknown, but can be prescribed in terms of known functions (which originated from lifting line theory) with unknown coefficients by the use of Multhopp's interpolation formula:

$$f_n(\eta') = \sum_{m=1}^M f_{nm} S_m(\theta') \quad (5)$$

where

$$f_{nm} = f_n(\eta_m)$$

$$\eta_m = \cos \theta_m = \cos \frac{m\pi}{M+1}$$

$$\theta' = \cos^{-1} \eta'$$

$$S_m(\eta') = \frac{(-1)^{m+1} \sin \theta_m \sin[(M+1)\theta']}{(M+1)(\eta' - \eta_m)} \quad (6)$$

Note that $S_m(\eta')$ is not singular (fig. 2). Substituting equations (4) to (6) into (3) leads to

$$\alpha(\xi, \eta) = \sum_{n=1}^N \sum_{m=1}^M f_{nm} \alpha_{nm}(\xi, \eta) \quad (7)$$

where

$$\alpha_{nm}(\xi, \eta) = \frac{-1}{8\pi} \int_{\xi_{le}}^{\xi_{te}} \int_{-1}^{+1} \frac{\Delta C_{p_{nm}}(\xi', \eta')}{(\eta' - \eta)^2} \bar{K}[\xi - \xi', \beta(\eta - \eta')] d\xi' d\eta' \quad (8)$$

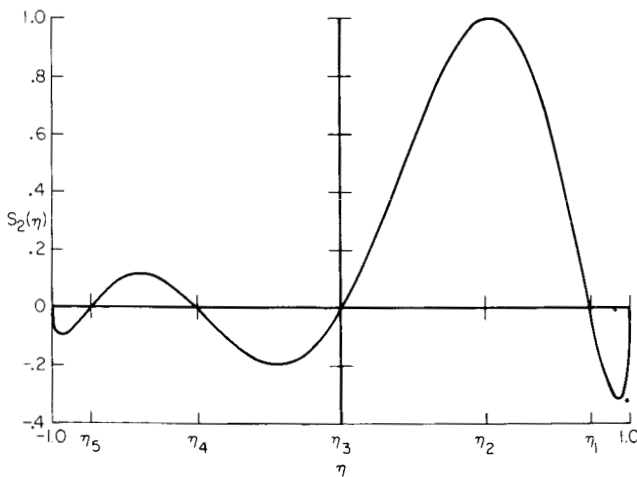


Figure 2.- Multhopp interpolation function of equation (6) for $M = 5$ and $m = 2$.

and

$$\Delta C_{p_{nm}}(\xi', \eta') = \frac{2b}{c(\eta')} h_n(\xi') S_m(\eta') \quad (9)$$

The final step in the basic solution is to determine the unknowns, f_{nm} , by enforcing equation (7) at a set of selected control points on the wing (collocation).

The α_{nm} 's are called downwash modes (or regular downwash modes). Because of the particular choices for the pressure modes given in equation (9), the resulting downwash modes are

smooth functions (except at spanwise stations where $c(\eta')$ is not continuous or differentiable). A moderate number of such downwash modes is inadequate to represent the discontinuous $\alpha(\xi, \eta)$ which would occur for a wing having a deflected control surface.

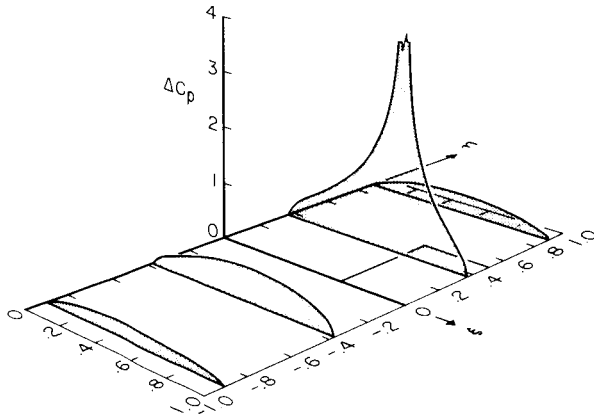


Figure 3.- Distribution of the flap mode of pressure on an aspect ratio 2 rectangular wing with a single flap; hinge line at $\xi = 0.65$ and edges at $\eta = 0$ and $\eta = 0.5$.

the flap, except possibly near the trailing edge. It has been determined that the pressure mode will produce the correct discontinuity at the trailing edge also. However, only the strength of the singular part of the pressure was determined by Landahl and a residual part remains to be determined. It is apparent then that the pressure mode need not contain any unknown elements nor be involved in a collocation procedure. The proper manner in which to employ Landahl's result is quite simple. Let the integral equation (eq. (3)) be symbolically denoted by

$$\alpha = \Delta C_p * K$$

Now let $\Delta C_p = \Delta C_{p_f} + \Delta C_{p_{pf}} - \Delta C_{p_{pf}}$, then

$$\begin{aligned} \alpha &= \Delta C_{p_f} * K + (\Delta C_p - \Delta C_{p_{pf}}) * K \\ &= \alpha_f + (\Delta C_p - \Delta C_{p_{pf}}) * K \end{aligned}$$

or

$$\alpha - \alpha_f = (\Delta C_p - \Delta C_{p_{pf}}) * K$$

The term α_f can be calculated since $\Delta C_{p_{pf}}$ is a known function and since α is given, $\alpha - \alpha_f$ (which could be termed a residual downwash) is completely known. The residual pressure distribution, $\Delta C_p - \Delta C_{p_{pf}}$, is unknown, but since $\alpha - \alpha_f$ is continuous (although it may not be differentiable at a flap edge), $\Delta C_p - \Delta C_{p_{pf}}$

The most obvious method of handling a discontinuous $\alpha(\xi, \eta)$ is to use the results of two-dimensional airfoil theory for a section with a flap (ref. 7) and lifting line theory for a discontinuous downwash distribution (ref. 8) to obtain an additional (flap) pressure mode in the form of equation (4). It was concluded in reference 9, however, that such a pressure mode cannot be made to reliably represent the partial span flap, and that pressure modes developed from three-dimensional theory are needed.

Landahl (ref. 1) developed such a pressure mode (fig. 3) for an unswept flap. He also showed that the pressure mode produces a downwash mode with exactly the required discontinuity at the leading and side edges of

should be sufficiently smooth that it may be expanded in the regular pressure modes. Consequently, the residual pressure may be determined with an existing lifting surface program, and the final pressure distribution is given merely by adding the flap pressure mode to the residual pressures. This is basically the method followed here. The most difficult part was the numerical integration procedure used to calculate the flap downwash distribution efficiently and accurately.

The procedures used are discussed in the next section in sufficient generality that they may be used to compute the downwash caused by any pressure mode. The actual form of the flap pressure mode used is discussed in appendix A.

BASIC INTEGRATION PROCEDURE

It was necessary to adopt an optimized quadrature procedure for the flap pressure mode for the following reasons:

(1) Evaluating the flap pressure mode at a single, given point is more difficult than for the regular pressure modes.

(2) The pressure is logarithmically singular at the hinge line. This necessitates an increased number of chordwise quadrature points.

(3) More spanwise integration points are needed than for regular pressure modes and, due to the second-order singularity in the spanwise integral, the number of chordwise integration points must be increased simultaneously. Therefore, if the number of spanwise integration points were doubled, the total number of integration points should be more than doubled (approximately tripled).

(4) The flap pressure is not in a separated form since it was derived from a three-dimensional analysis. Therefore, the pressure at each point must be calculated directly and cannot be represented as a simple product of previously calculated and stored values, that is, the matrix of the flap pressure mode values is not the outer product of two vectors as it is for the regular pressure modes. Consequently, the time required to perform a calculation for the flap pressure mode is much greater than for a regular pressure mode and therefore more efficient quadrature procedures are desirable.

To best explain these procedures, consider first the spanwise integration. The flap downwash mode or any regular downwash mode can be manipulated into the following form:

$$\alpha_f(\xi, \eta) = \frac{-1}{2\pi} \int_{-1}^{+1} \frac{G_f(\xi, \eta, \eta')}{(\eta - \eta')^2} d\eta' \quad (10)$$

where G_f is the result of a chordwise numerical integration that has already been performed and may contain some error. The integration indicated by equation (10) may be performed by various methods; the one used in this report is from Multhopp (ref. 2; see appendix B also), but the general procedure for

obtaining an efficient method would be similar for other choices of the spanwise integration technique. From reference 2, the following approximation is obtained for equation (10):

$$\alpha_f(\xi, \eta) = \sum_{j=1}^J b_j(\eta) G_f(\xi, \eta, \eta_j) \quad (11)$$

where

$$\eta_j = \cos \theta_j$$

and

$$\theta_j = \frac{j\pi}{J+1}$$

If η is restricted to

$$\eta = \cos \frac{v\pi}{J+1}$$

where v is some integer, then the expression for $b_j(\eta)$ is

$$b_j(\eta) = \begin{cases} \frac{J+1}{4 \sin \theta_j}, & v = j \\ \frac{-\sin \theta_j}{(J+1)(\eta - \eta_j)^2}, & |v-j| \text{ odd} \\ 0, & \text{otherwise} \end{cases} \quad (12)$$

Nonzero values of $b_j(\eta)$ for various choices of J are given in figure 4. Note that the coefficients become very large for the integration stations nearest η .

Consider the application of equations (11) and (12) for $\eta = 0$:

$$\alpha_f(\xi, 0) = \frac{J+1}{4} G_f(\xi, 0, 0) - \frac{1}{J+1} \sum_{j=1, J, 2} \frac{\sin \theta_j}{(\eta_j)^2} G_f(0, \xi, \eta_j)$$

Recall that G_f is the result of a chordwise integration subject to some error and assume, for illustration, that it is calculated exactly at all η_j except $j = v-1$, where the magnitude of the error is δG_f .

Then the magnitude of the error in computing α_f is

$$\delta \alpha_f = \frac{-\sin \theta_{v-1}}{(J+1)(\eta_{v-1})^2} \delta G_f$$

which, for moderate or large J , is approximately

$$\delta\alpha_f \approx -\frac{J+1}{\pi^2} \delta G_f \quad (13)$$

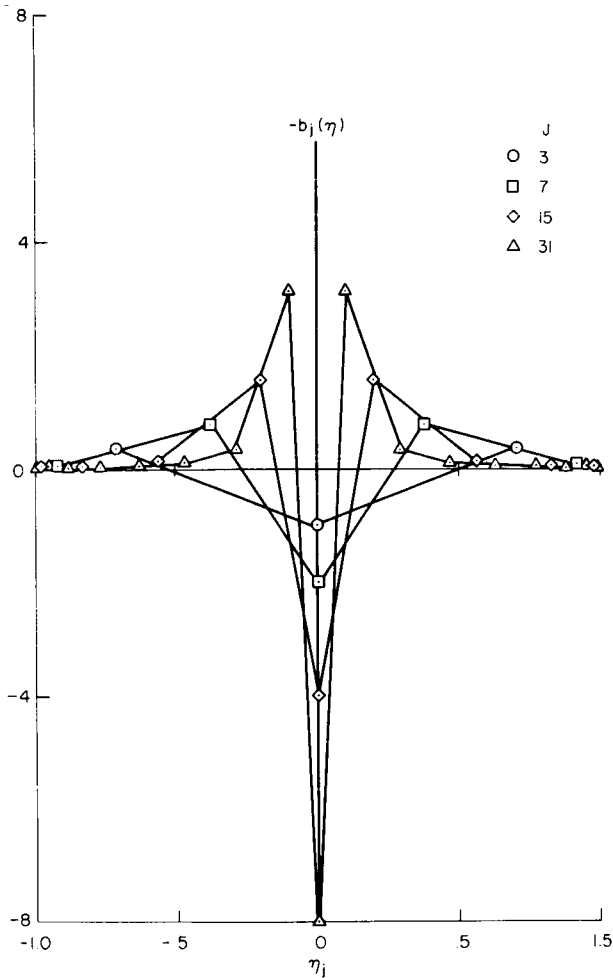


Figure 4.- Quadrature coefficients for the downwash integral $\eta = 0$.

Thus, by increasing J , the value obtained for $\alpha_f(\xi, 0)$ does not converge to the correct answer, but, on the contrary, diverges from it.

A good example of this type of instability is given by Rowe (ref. 10). He calculated the lift-curve slope of a square wing using various numbers of chordwise and spanwise integration points. When he used 4 chordwise points and increased the number of spanwise points beyond 12, his results diverged, whereas with 13 chordwise points the results were stable when the number of spanwise points was increased to 16. If Rowe had continued increasing the number of spanwise integration stations without increasing the number of chordwise points, however, his results would have again become unstable.

It follows from the discussion relating to equation (13) that, to guarantee convergence, the chordwise integration that determined G_f should use enough points so that

$$\delta G_f < \frac{\epsilon(\xi, 0, \eta_{v-1})}{(J+1)^P} \quad (14)$$

where P is a constant greater than 1 (a value of 2 is used here).

In effect, equation (14) is satisfied typically by selecting the largest value of J likely to be used (or some equivalent to J if a quadrature rule other than that given by eqs. (11) to (12) is employed) and then using enough chordwise quadrature points to ensure an acceptably accurate result. An obvious drawback to this approach is that if a smaller value of J were used, more chordwise points would be used than necessary. Another, and more important, drawback is that actually determining the number of chordwise points to use requires considerable experimentation even for the regular pressure modes. (An example of this is provided in appendix B, figure 1 of ref. 11.) Since the flap pressure mode contains additional parameters, such experimentation was not considered practical. Another method for determining the number of chordwise integration points was needed.

The method used is as follows: The chordwise integration is performed repeatedly with an increasing number of points and the difference obtained with each increase is compared until it is less than some prescribed value, δ . The difference is approximately proportional to the actual error (when $|\eta - \eta'|$ is very small this is not always true and additional considerations are necessary). Consequently, the actual error can be controlled by specifying δ . This procedure would be inefficient except that it is possible to nest the quadrature rules so that the number of arithmetic computations performed is only slightly greater than the number that would have been performed if the computation had been done only with the final number of integration points. Consider the chordwise integrals, which can be put in the following form:

$$G_f(\xi, \eta, \eta_j) = \int_{-1}^{+1} \sqrt{1-x'^2} h(x', \eta, \eta_j) dx' \quad (15)$$

The above integral is evaluated by the Gaussian quadrature rule having $\sqrt{1-x'^2}$ as its weight function on the interval $(-1, +1)$:

$$G_f(\xi, \eta, \eta_j) \approx \frac{\pi}{M+1} \sum_{m=1, M} \sin^2 \frac{m\pi}{M+1} h\left(\cos \frac{m\pi}{M+1}, \eta, \eta_j\right) \quad (16)$$

Equation (16) shows that if G_{f_n} results from using M_n points, then

$$G_{f_{n+1}} = \frac{1}{2} G_{f_n} + \frac{\pi}{M_{n+1} + 1} \sum_{m=1, M_{n+1}, 2} \sin^2 \frac{m\pi}{M_{n+1} + 1} h\left(\cos \frac{m\pi}{M_{n+1}}, \eta, \eta_j\right) \quad (17)$$

if

$$M_{n+1} = 2M_n + 1$$

Thus, for example, one can obtain the result of using 15 integration points by computing function values at only 8 points and using also the result obtained with 7 points. One would then have the results of using 15 and 7 points (and hence information on the convergence) with only slightly more effort than would be involved in obtaining the answer for 15 points only.

Now that the method whereby stability can be assured with respect to increasing the number of spanwise integration points (as exemplified by eq. (14)) and the method for controlling the accuracy of the chordwise integration has been discussed, it is appropriate to consider how to minimize the total error for a fixed number of spanwise integration points while holding the total number of integration points constant. In doing this, some crude approximations must be introduced. However, the equations representing the approximations will be eliminated so that the results will be essentially independent of them. The only effect of the approximations would be to control the total number of integration points used in obtaining the downwash values, that is, the procedure may not actually be fully optimized, but the results will be accurate.

The application of equation (11) gives

$$|\delta\alpha_f| \leq \sum_{j=1, J} |b_j| \delta G_{fj} \quad (18)$$

The right-hand side is to be minimized with respect to variations of the number of chordwise points used at each station, M_j , subject to the constraint that the total number of integration points used be constant, that is,

$$M = \sum_{j=1, J} M_j \quad (19)$$

should be constant. Lagrange's multiplier method gives the following equations for M_j :

$$|b_j| \frac{\partial \delta G_f}{\partial M_j} + \lambda = 0 \quad (20)$$

Here the approximation previously discussed is introduced, namely,

$$\delta G_f \sim \frac{|b_j|^q}{M_j^r} \quad (21)$$

where $q, r = \text{constants} > 0$. It is only reasonable that δG_f decrease as M_j increases. The effect of b_j on the error occurs because the error obtained with a given number of chordwise integration points increases with decreasing distance of the control point from the integration point due to the nature of

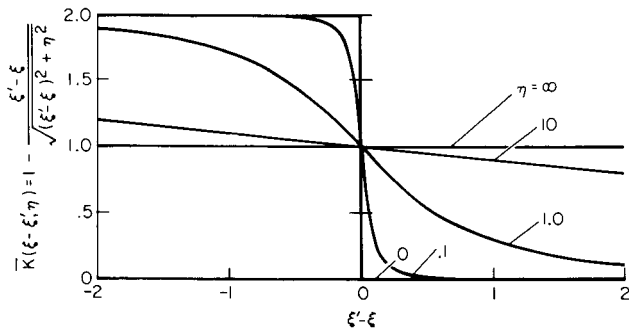


Figure 5.- Illustration of the discontinuity of the function \bar{K} (eqs. (2) and (11b)).

\bar{K} in equation (2) and figure 5. The quadrature weights b_j also increase in magnitude as the integration point approaches the control point. Thus, $|b_j|$ is a measure of this distance effect (even though it may be imprecise) and this explains its appearance in equation (21).

The use of equation (21) in (20) then gives

$$\frac{|b_j|^{q+1}}{|M_j|^{r+1}} \sim \text{const}$$

using equation (21) again gives

$$\delta G_f |b_j|^{(q+1) \frac{r}{r+1} - q} \sim \text{const} \quad (22)$$

The values of q and r have not been separately studied, only their combination as given in equation (22). A value of $1/2$ (values of 0 , $1/2$, and 1 were used) gives the most accurate answers for a given total number of integration points.

At this point it would be beneficial to summarize the concepts presented thus far:

(1) The chordwise integral is done with an increasing number of chordwise points using nested quadrature rules for efficiency until the resulting differences are less than a prescribed value, δ .

(2) To use the fewest total number of integration points for a given number spanwise, δ is taken to be inversely proportional to the square root of the absolute value of the associated quadrature weight.

(3) For convergence with respect to the number of spanwise integration points, δ is taken to be inversely proportional to $(J+1)^2$, thus

$$\delta = \frac{\delta_0}{|b_j|^{1/2}(J+1)^2} \quad (23)$$

Note that the error involved in applying this procedure is highly independent of any specific planform. The effect of planform changes is to change the number of chordwise integration points needed to actually achieve the δ given by equation (23) and to change the number of spanwise integration points needed to make equation (11) an accurate approximation of equation (10). It is therefore possible to prescribe δ_0 for all planforms, leaving J as the only parameter that must be varied to account for planform changes. Furthermore, since it is possible to nest the spanwise quadrature rules in a manner similar to that used in the chordwise integration, downwash modes computed with various values of J can be determined simultaneously. This allows a rapid determination of whether the largest value of J used was sufficiently large. Thus, multiple computer runs to assess the effect of J are usually unnecessary.

ILLUSTRATIVE COMPUTATIONS AND COMPARISONS

This method for treating partial span flaps has been used with an extended version of Wagner's lifting surface computer program (ref. 6) to compute pressures, span loading, and control surface derivatives on various configurations. The primary extensions made to this program (hereafter referred to as WAGNG) were: (1) to allow use of an arbitrary number of chordwise control points (Dr. Wagner's extension) and (2) to allow use of an arbitrary downwash distribution. In this program, a total of N lateral control lines are placed on the wing leading and trailing edges and at the chordwise locations (given by eq. (A12)) and M streamwise control lines are distributed at the Multhopp locations (given by η_m of eq. (5)). The intersections of these lines are the control points, where the boundary conditions are enforced. The number of control points is $N \times M$, but symmetry or antisymmetry is used to reduce the actual number of unknowns to about half that value. Before discussing any final results, however, the character of the residual downwash should be examined.

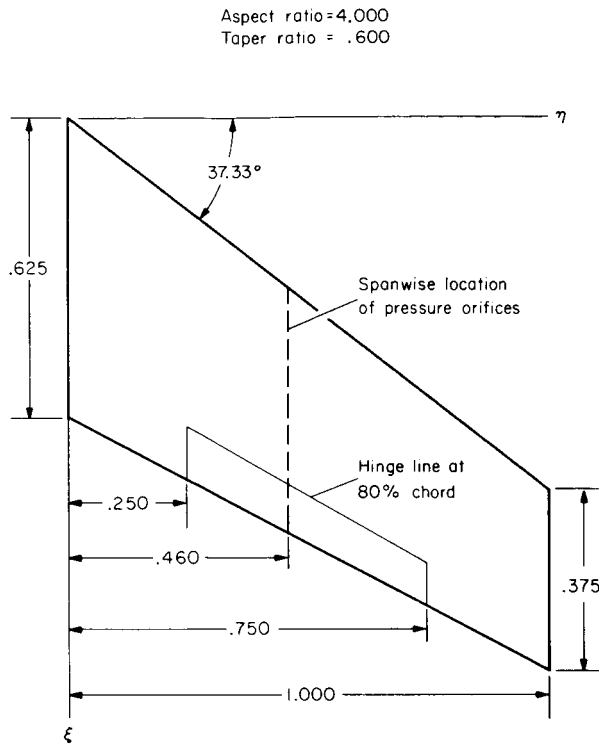


Figure 6.- Relative dimensions of the wing tested in reference 12.

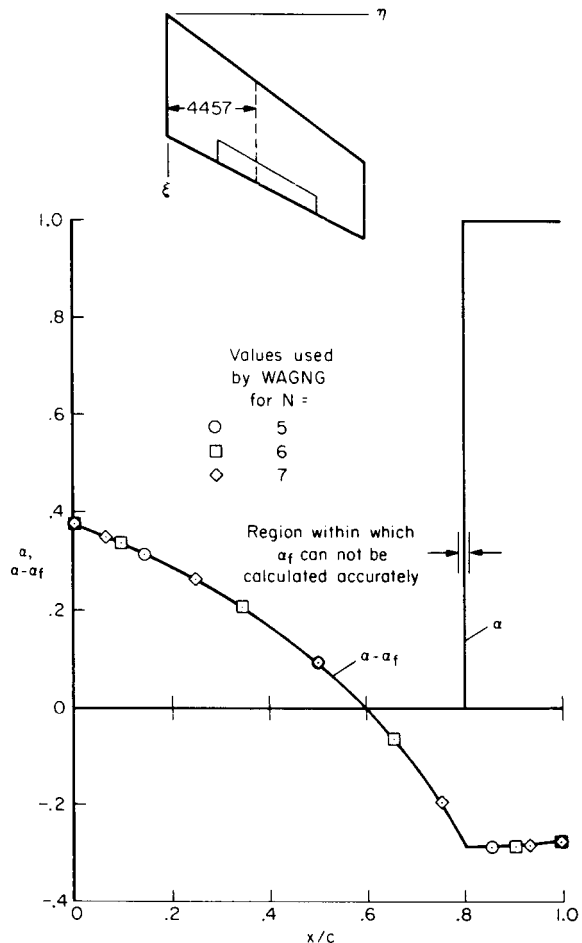


Figure 7.- Chordwise distribution of given and residual downwash at $\eta = 0.4457$.

Figure 6 shows the planform of a wing (ref. 12) for which detailed computations of the residual downwash were performed. A chordwise distribution of the given downwash, α , and the residual downwash, $\alpha - \alpha_f$, are shown in figure 7. Note that $\alpha - \alpha_f$ has a discontinuous derivative at the hinge line which could probably be eliminated, but the distribution is felt to be smooth enough for most purposes. Within 1-percent c of the hinge line, α_f cannot be calculated accurately with the present computer program because of a limitation on the maximum number of spanwise integration points (543). The number of chordwise control stations can be chosen to avoid the necessity of computing in this region, however. As shown in reference 13, there are similar regions near, but excluding, the wing edges. The latter regions are small enough that they have caused no problem for $N < 9$ (the maximum number of chordwise control stations allowed by WAGNG). Figure 7 also shows the chordwise control stations used for several values of N and corresponding values of $\alpha - \alpha_f$ given to the lifting surface program.

Spanwise distributions of α and $\alpha - \alpha_f$ are shown in figure 8. The discontinuities in the derivative of $\alpha - \alpha_f$ at the side edges could probably be

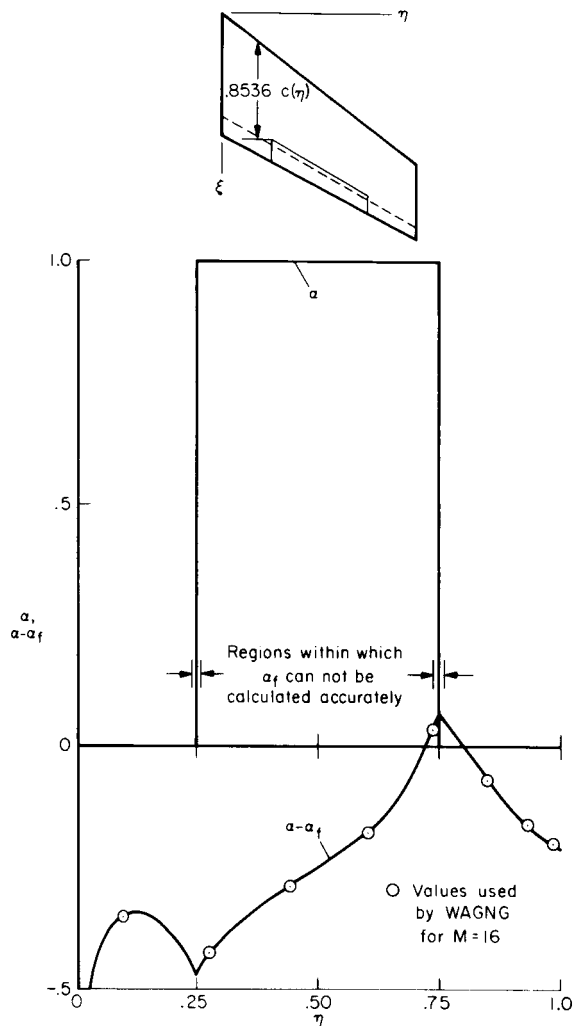


Figure 8.- Spanwise distribution of given and residual downwashes at the chordwise station $x/c = 0.8536$.

strength were used on the semispan. WAGNG with $N = 7$ and $M = 16$ used 56 unknowns (although a comparable result was obtained with $N = 5$ and thus 40 unknowns). The theoretical results agree reasonably well with experiment except aft of the hinge line, where the influence of viscosity is strong.

Figure 11 shows a predicted section lift coefficient distribution for a 10° flap deflection on an $AR = 8.56$ swept wing. It is compared with experimental values and values predicted by a vortex lattice method for a nearly identical wing (ref. 15). The difference between the theoretical methods is small, but both differ considerably from the experimental values. Reference 15 suggests that a possible reason for this may be separated flow since the data were taken at a wing angle of attack of 10° and thus the flap was actually at 20° incidence.

eliminated also but, again, it is felt that this distribution is smooth enough for practical purposes. This figure also shows the singularity in downwash which will generally occur at any station for which the local sweep angle changes abruptly (in this case, at $\eta = 0$). This singularity occurs for the regular pressure modes (eq. (4)) also and the only way it has been eliminated is by introducing artificial rounding to the planform. However, if control points are not placed at or very near this point, no serious difficulties seem to arise and, apparently, the use of rounding is unnecessary. This is the approach that has been used here. Figure 8 also shows the values of $\alpha - \alpha_f$ actually used in WAGNG for the fourth ($N = 5$) chordwise control station ($x/c = 0.8536$) at the 8 spanwise control stations used for $M = 16$.

Chordwise residual pressure distributions calculated by WAGNG from $\alpha - \alpha_f$ are shown in figure 9 for $M = 16$ and $N = 5, 6,$ and 7 . The differences are minor and support the previous statement that eliminating the discontinuous derivative of $\alpha - \alpha_f$ is not necessary for practical purposes.

Calculated and experimental results are compared in figure 10. The constant pressure panel calculation was performed by Ralph Carmichael of Ames Research Center using a version of the Ames Wing-Body Computer Program (ref. 14). Two-hundred panels of unknown

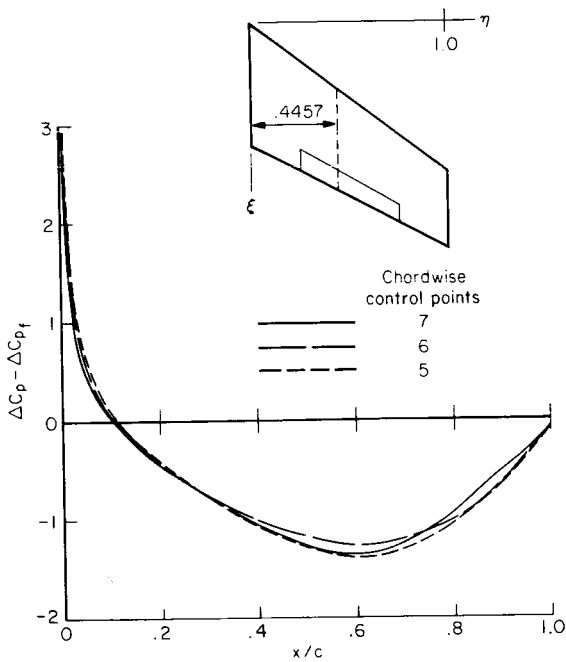


Figure 9.- Comparison of residual chordwise pressure distributions calculated by the Wagner computer program from the residual downwash $\alpha - \alpha_f$; $\eta = 0.4457$.

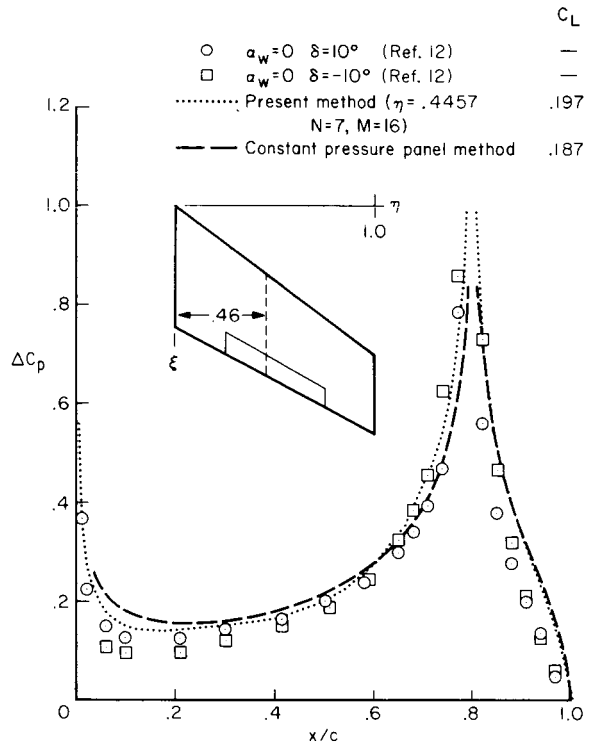


Figure 10.- Comparison of experimental and calculated lifting pressure distributions on a swept wing with partial span flap; $M = 0.6$, $\eta = 0.46$.

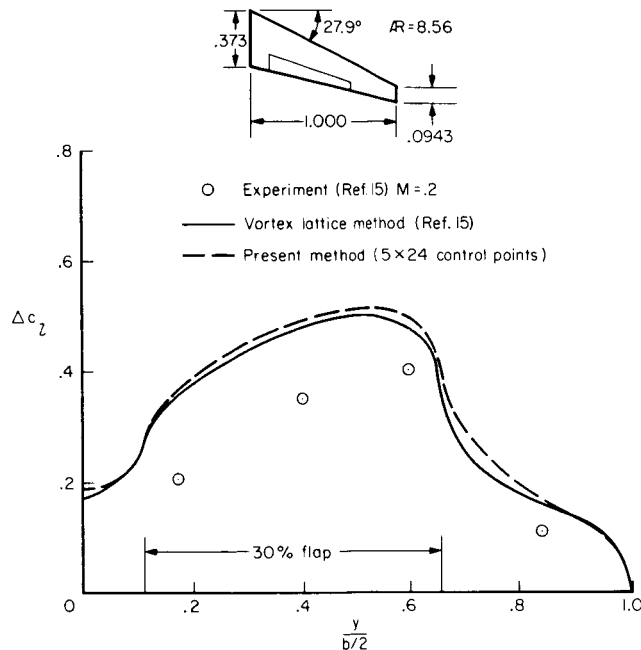


Figure 11.- Comparison of calculated and experimental section lift coefficient distributions for a wing with a partial span flap.

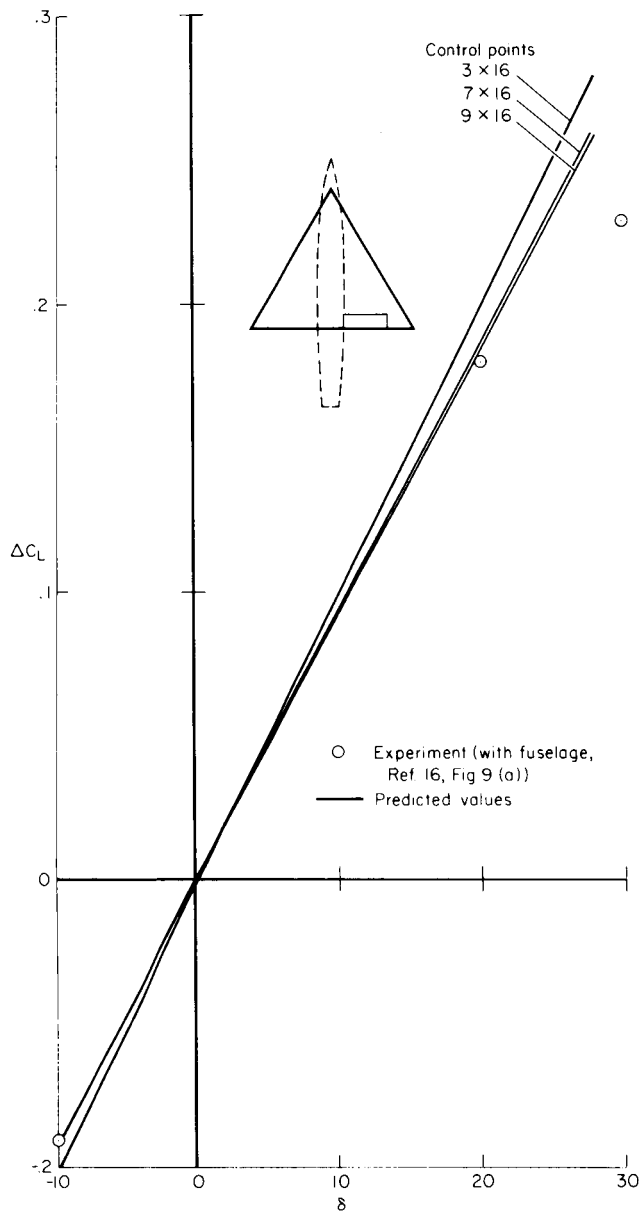


Figure 12.- Comparison of predicted and experimental ΔC_L for a 60° delta wing.

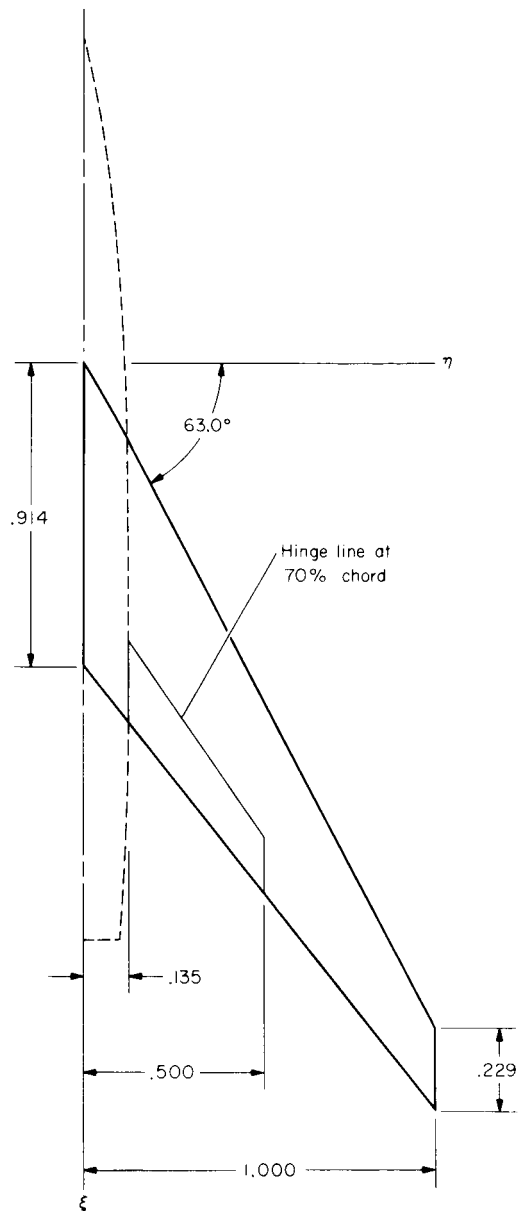


Figure 13.- Wing tested in reference 17.

A third comparison is given in figure 12, where ΔC_L induced by flap deflection on a 60° delta wing is shown as a function of angle of attack. A sufficiently accurate answer was obtained with $N = 7$, with the predicted slope only 3 percent above the experimental value (ref. 16). This close agreement, however, may not be the result of a good theory, but more likely because the theory ignores the presence of the fuselage, which acts somewhat as a reflection plane and thus would tend to increase $C_{L\delta}$. This phenomenon is also apparent in the next comparison.

Figure 13 shows the planform of this next example (ref. 17). The Mach number variations of the predicted and experimental control surface derivatives,

$C_{L\delta}$, $C_{H\delta}$, and $C_{\ell\delta}$, are shown in figures 14 through 16, respectively (the theory is invalid at $M = 0.9$, however, since this is above the critical Mach number). The term $C_{L\delta}$ is actually underpredicted by 5 percent (8×24 control points at $M = 0.6$), which, as mentioned above, results from not accounting for the interference of the fuselage. The term $C_{H\delta}$ is overpredicted by 15 percent ($M = 0.6$). Had the body interference been accounted for, the discrepancy might have been greater; this discrepancy is large (and expected) since $C_{H\delta}$ depends only on the lifting pressure in the region most adversely affected by viscosity. The rolling moment derivative, $C_{\ell\delta}$, is underpredicted by 6.5 percent ($M = 0.6$).

The comparisons presented here indicate that the present method can predict with reasonable accuracy features of the flow about wings with deflected control surfaces. However, this linearized theory will fail when there is separated flow, and this happens more readily when a control surface is deflected. Consequently, the method should be used with discrimination. The comparisons also indicate that finite element methods can predict flow features for this type of configuration. However, a method of the present type (i.e., employing continuous loading functions) can be made more economical since far fewer unknowns are needed.

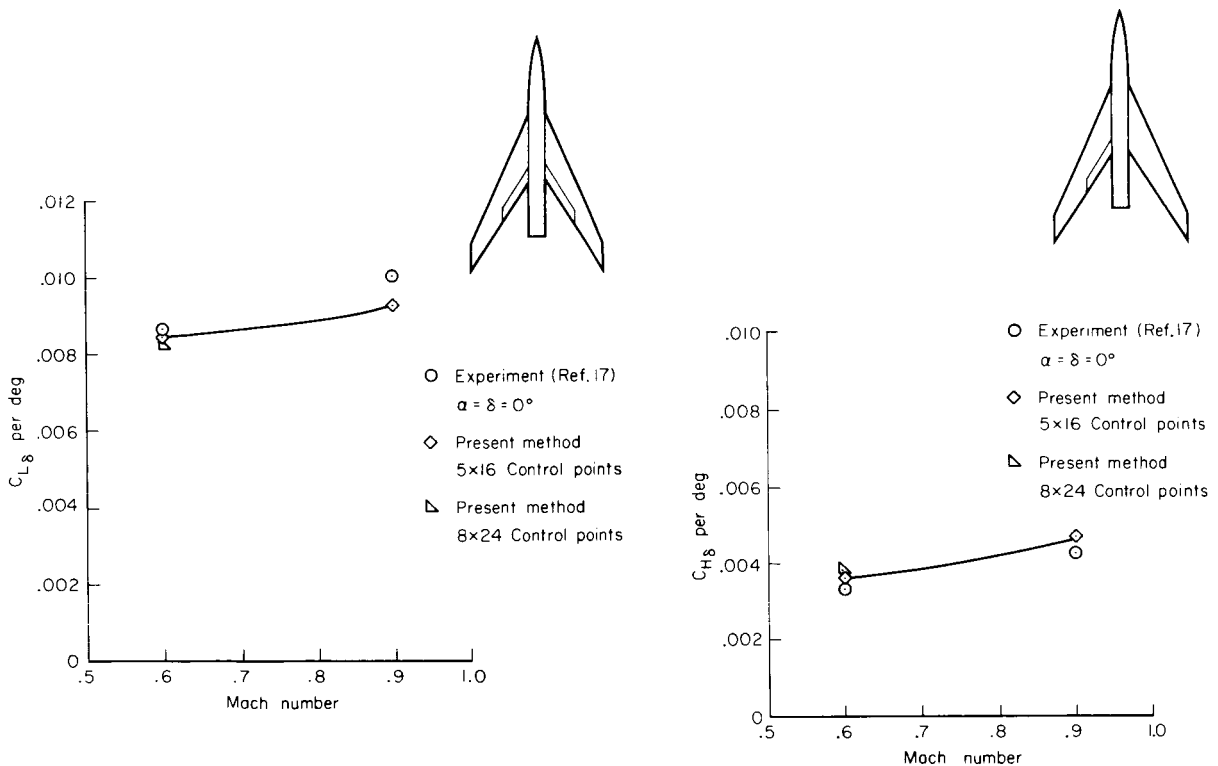


Figure 14.- Variation of control surface lift effectiveness with Mach number (symmetric deflection of two surfaces).

Figure 15.- Variation of the $C_{H\delta}$ hinge moment coefficient with Mach number (one surface only).

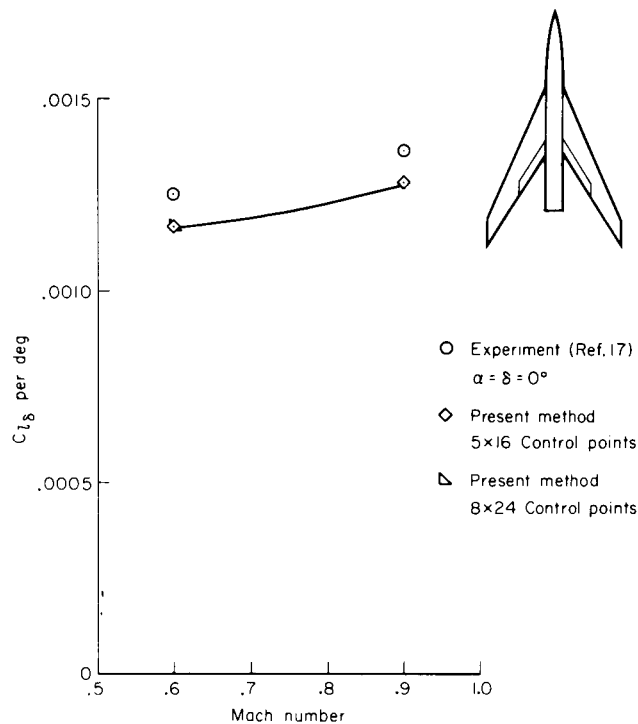


Figure 16.- Variation of control surface rolling moment effectiveness with Mach number (antisymmetric deflection of two surfaces).

CONCLUDING REMARKS

The governing integral equation of linearized, steady lifting surface theory was examined and a standard method for solving it, based on infinite aspect ratio theory, was briefly reviewed. It was pointed out that to treat the partial span flap, one should not proceed similarly from the corresponding infinite aspect ratio theory but rather use a three-dimensional local solution (ref. 1) because only the latter can reliably represent the pressure distribution near the control surface corner. This local solution was incorporated with an existing lifting surface program to obtain a complete solution to the problem.

Next a basic procedure for performing the numerical quadratures required was derived. The results were in no way related to the fact that a control surface pressure mode was being used, so they actually bear a direct significance to lifting surface theory in general. It was determined how instabilities in the spanwise integration occur if the chordwise and spanwise integration procedures are not coupled. The manner in which the integration procedure should be related required the chordwise integration to be performed with a specified accuracy, depending on the spanwise integration and control stations. It was indicated that the usual procedures are necessarily inefficient in attaining the required accuracy. A new method was introduced which is more

efficient because it does not compute to a greater accuracy than needed and, furthermore, because it uses the concept of "nested" quadrature rules.

Following the discussion of the quadrature procedures, illustrative computations and comparisons with experiments were discussed. The nature of the control surface downwash mode was shown to be such that the discontinuity in the given downwash could be properly eliminated, but discontinuous derivatives remained. Calculated examples showed, however, that these irregularities are sufficiently weak so as not to constitute a real problem. The method presented was demonstrated to be an effective, accurate solution to the integral equation. However, in some cases there were rather large discrepancies with experiments. This was not unexpected. The principal causes were viscosity and the neglect of body and thickness interference effects. Also, another possible source of discrepancy is the gap between the control surface side edges and the wing due to the control surface's deflection. This gap is not accounted for in the theory.

Ames Research Center

National Aeronautics and Space Administration

Moffett Field, Calif. 94035, July 26, 1972

APPENDIX A

FORM OF THE FLAP PRESSURE MODE AND CHORDWISE INTEGRATION

The flap downwash mode is given by

$$\alpha_f(\xi, \eta) = \frac{-1}{8\pi} \int_{-1}^{+1} \int_{\xi_{le}}^{\xi_{te}} \frac{\Delta C_p}{(\eta' - \eta)^2} \bar{K}[\xi - \xi', \beta(\eta - \eta')] d\xi' d\eta' \quad (A1a)$$

where

$$\bar{K}[\xi - \xi', \beta(\eta - \eta')] = 1 + \frac{\xi - \xi'}{\sqrt{(\xi - \xi')^2 + \beta^2(\eta - \eta')^2}} \quad (A1b)$$

This can be put in a more convenient form by the use of the following transformations:

$$\xi = [\xi_{te}(\eta') - \xi_{le}(\eta')] \frac{1+x}{2} + \xi_{le}(\eta') \quad (A2a)$$

$$\xi' = [\xi_{te}(\eta') - \xi_{le}(\eta')] \frac{1+x'}{2} + \xi_{le}(\eta') \quad (A2b)$$

then

$$\alpha_f(\xi, \eta) = \frac{-1}{8\pi} \int_{-1}^{+1} \frac{c(\eta')}{(\eta' - \eta)^{2b}} \left[\int_{-1}^{+1} \Delta C_p \bar{K}(x-x', y) dx' \right] d\eta' \quad (A3)$$

where

$$y = \frac{b\beta}{c(\eta')} (\eta - \eta')$$

Expressions for ΔC_p were given by Landahl and extended by Ashley (ref. 18) to the case of a swept flap. The expression given below (for unit flap deflection) has been adapted from these references with a correction made to properly account for the flap edges:

$$\Delta C_p = \frac{-2 \cos \lambda_c}{\pi \sqrt{1-M^2} \cos^2 \lambda_c} F(x', \eta') \ln \left[\frac{\sqrt{(x' - x_c)^2 + y_1^2} - y_1}{\sqrt{(x' - x_c)^2 + y_2^2} - y_2} \right] \quad (A4a)$$

where

$$y_1 = \frac{b}{c(\eta')} \frac{\sqrt{1 - M^2} \cos^2 \lambda_c}{\cos \lambda_c} c (\eta' - \eta_1) \quad (A4b)$$

$$y_2 = \frac{b}{c(\eta')} \frac{\sqrt{1 - M^2} \cos^2 \lambda_c}{\cos \lambda_c} c (\eta' - \eta_2) \quad (A4c)$$

The function $F(x', \eta')$ must attain a value of 1.0 on the flap hinge line and must introduce the correct edge behavior on the periphery of the planform (ref. 1), but is otherwise arbitrary. It has been chosen to be the following:

$$F(x', \eta') = C_2(\eta') \sqrt{\frac{1 - x'^2}{1 - x_c^2}} \quad (\text{A4d})$$

where

$$C_2(\eta') = \begin{cases} 1 & |\eta'| \leq \eta_2 \\ \sqrt{1 - \left(\frac{|\eta'| - |\eta_2|}{1 - |\eta_2|}\right)^2} \left[1 + \frac{1}{2} \left(\frac{|\eta'| - |\eta_2|}{1 - |\eta_2|}\right)^2 \right] & |\eta'| > |\eta_2| \end{cases} \quad (\text{A4e})$$

Combining equations (A3) and (A4) yields

$$\alpha_f(\xi, \eta) = \frac{\cos \lambda_c}{4\pi^2 \sqrt{1-M^2} \cos^2 \lambda_c} \int_{-1}^{+1} \frac{C_2(\eta') \frac{c(\eta')}{b}}{(\eta' - \eta)^2} H_f(\xi, \eta, \eta') d\eta' \quad (\text{A5a})$$

where

$$H_f(\xi, \eta, \eta') = \int_{-1}^{+1} \sqrt{1-x'^2} g(x') dx' \quad (\text{A5b})$$

and

$$g(x') = \frac{1}{\sqrt{1-x_c^2}} \ln \left[\frac{\sqrt{(x'-x_c)^2 + y_1^2} - y_1}{\sqrt{(x'-x_c)^2 + y_2^2} - y_2} \right] \bar{K}(x-x', y) \quad (\text{A5c})$$

As indicated previously, the function H_f may have to be calculated very accurately and it is to be calculated by the following Gaussian quadrature rule:

$$\int_{-1}^{+1} \sqrt{1-x'^2} g(x') dx' = \frac{\pi}{J+1} \sum_{j=1, J} (1-x_j^2) g(x_j) \quad (\text{A6a})$$

where

$$x_j = \cos \frac{j\pi}{J+1} \quad (\text{A6b})$$

For equation (A6a) to be accurate, the function $g(x')$ should be able to be expressed accurately as a polynomial of degree less than $2J$. Accordingly, the logarithmic singularity of $g(x')$ at x_c when Y_1 and Y_2 are of opposite sign or when Y_1 or Y_2 is zero must be eliminated or at least softened. Similarly, the discontinuity that \bar{K} has at $x' = x$ when $y = 0$ must be softened. The former has been accomplished with the following function:

$$\bar{g}(x') = g(x') - \frac{\sqrt{1-x'^2}}{\sqrt{1-x_c^2}} \ln \left[\frac{\sqrt{(x'-x_c)^2 + y_1^2} - y_1}{\sqrt{(x'-x_c)^2 + y_2^2} - y_2} \right] \bar{K}(x-x_c, y) \quad (A7)$$

which is not singular anywhere, but has singular derivatives at $x' = \pm 1$ and $x' = x_c$, but these are much less serious. The influence function is then given by

$$\begin{aligned} H_f(\xi, \eta, \eta') &= \frac{\pi}{J+1} \sum_{j=1, J} (1-x_j^2) \bar{g}(x_j) \\ &+ \frac{\bar{K}(x-x_c, y)}{1-x_c^2} \int_{-1}^{+1} (1-x'^2) \ln \left[\frac{\sqrt{(x'-x_c)^2 + y_1^2} - y_1}{\sqrt{(x'-x_c)^2 + y_2^2} - y_2} \right] dx' \\ &= \frac{\pi}{J+1} \sum_{j=1, J} (1-x_j^2) \bar{g}(x_j) \\ &+ \frac{\bar{K}(x-x_c, y)}{1-x_c^2} \left\{ \frac{x'-x_c}{3} (3-x_c^2 - x'x_c - x'^2) \ln \left[\frac{\sqrt{(x'-x_c)^2 + y_1^2} - y_2}{\sqrt{(x'-x_c)^2 + y_2^2} - y_2} \right] \right. \\ &+ y_1 \left[\sqrt{(x'-x_c)^2 + y_1^2} \left(\frac{5x_c + x'}{6} \right) - \left(1-x_c^2 + \frac{y_1^2}{6} \right) \ln \left[x'-x_c + \sqrt{(x'-x_c)^2 + y_1^2} \right] \right. \\ &\left. \left. - y_2 \left[\sqrt{(x'-x_c)^2 + y_2^2} \left(\frac{5x_c + x'}{6} \right) - \left(1-x_c^2 + \frac{y_2^2}{6} \right) \ln \left[x'-x_c + \sqrt{(x'-x_c)^2 + y_2^2} \right] \right] \right\} \Big|_{-1}^{+1} \quad (A8) \end{aligned}$$

When $y = 0$ and $|x| \neq 1$, there is a discontinuity within the integration interval (fig. 5). The previous procedure leads to the following expression for H_f :

$$H_f = \int_{-1}^x \sqrt{1-x'^2} \bar{g}(x') dx + \frac{\bar{K}(x-x_c, 0)}{1-x_c^2} \{ \text{same as in (A8) . . .} \} \Big|_{-1}^x \quad (A9)$$

The numerical integration is accomplished by substituting

$$\bar{g}(x') = \begin{cases} \bar{g}(x') - \bar{g}(x) - (x'-x)\bar{g}'(x) & x' < x \\ 0 & x' \geq x \end{cases} \quad (A10)$$

This function is suitably smooth to be integrated by the Gaussian quadrature method, resulting in:

$$H_f(\xi, \eta, \eta') = \frac{\pi}{J+1} \sum_{j=1, J} (1-x_j^2) \bar{g}(x_j) + \bar{g}(x) [x\sqrt{1-x^2} + \sin^{-1}x + \frac{\pi}{2}]$$

$$-\bar{g}'(x) \left[\frac{2+x^2}{3} \sqrt{1-x^2} + x(\sin^{-1}x + \frac{\pi}{2}) \right] + \text{last term in (A9)}$$

(A11)

In the above formula, note that the summation need not be performed for $x_j \geq x$ and that $\bar{g}(x) = \bar{g}'(x) = 0$ if $x < x_c$.

A question deserving consideration is whether there is a best choice for the number of quadrature points, J . Consider the function $\bar{K}(x-x', y)$ (see fig. 5). For small values of y , $\bar{K}(x-x', y)$ is nearly discontinuous at $x-x' = 0$, where it attains an average value. It seems obvious that an integration point at $x' = x$ would be desirable since some of the errors could then be made to cancel. The lifting surface program with which this method is used has (for small Y) the control points at $x \approx \pm 1$ and

$$x \approx \cos \frac{p\pi}{N-1} \quad p = 1, 2, \dots, N-2$$

(A12)

From equation (A6b), then, appropriate values for J would be

$$J = (N+1)^k - 1$$

(A13)

where k is any integer.

A final point to mention is that the procedures given for determining $H_f(\xi, \eta, \eta')$ may also be used to determine the flap pressure mode contribution to the section coefficients of lift and pitching moment about the quarter-chord merely by replacing \bar{K} with 1 and with $x'-0.5$, respectively. For this computation, however, there is no optimum value for J .

APPENDIX B

CORRECTIONS FOR THE LOGARITHMIC SINGULARITY AND OTHER SINGULARITIES
IN THE SPANWISE INTEGRAL

The spanwise integral for the flap downwash mode contains a factor of the form

$$H(\xi, \eta, \eta') = \int_{-1}^{+1} h(x', \eta') \left[1 + \frac{x-x'}{\sqrt{(x-x')^2 + y^2}} \right] dx' \quad (B1)$$

where $h(x', \eta')$ is a function that behaves as $\sqrt{1-x'^2}$ near the end points and that may have a logarithmic singularity. Assume, however, that in the vicinity of $x' = x$ it is a regular function. By developing $h(x', \eta')$ in a Taylor series it can be shown that $H(\xi, \eta, \eta')$ has a logarithmically singular second derivative. Only the contribution in the vicinity of $x' = x$ need be considered:

$$\begin{aligned} H(\xi, \eta, \eta') &= \int_{x-\delta}^{x+\delta} h(x', \eta') \frac{x-x'}{\sqrt{(x-x')^2 + y^2}} dx' + \text{a regular part} \\ &= \int_{x-\delta}^{x+\delta} \left\{ h(x, \eta') + (x'-x) \frac{\partial h}{\partial x'}(x, \eta') + \dots \right\} \frac{x-x'}{\sqrt{(x-x')^2 + y^2}} dx' \\ &\quad + \text{a regular part} \\ &= \int_{-\delta}^{+\delta} \left\{ \frac{\partial h}{\partial x'}(x, \eta') \bar{x} + \dots \right\} \frac{-\bar{x}}{\sqrt{\bar{x}^2 + y^2}} d\bar{x} + \text{a regular part} \\ &= -2 \frac{\partial h}{\partial x'}(x, \eta') \left[\frac{\bar{x}}{2} \sqrt{\bar{x}^2 + y^2} - \frac{y^2}{2} \ln(\bar{x} + \sqrt{\bar{x}^2 + y^2}) \right] \Big|_{-\delta}^{\delta} \\ &\quad + \text{a regular part} + \text{lower-order singularities} \\ &= - \frac{\partial h}{\partial x'}(x, \eta') y^2 \ln|Y| + \text{a regular part} \\ &\quad + \text{lower-order singularities} \\ &= - \frac{\partial h}{\partial x'}(x, \eta') \left[\frac{b\beta}{c(\eta')} \right]^2 (\eta - \eta')^2 \ln|\eta - \eta'| + \text{a regular part} \\ &\quad + \text{lower-order singularities} \end{aligned} \quad (B2)$$

The factor $(\eta - \eta')^2$ is cancelled by its reciprocal in the spanwise integral, leaving a logarithmic singularity. This singularity also exists for the regular downwash modes and was recognized by Multhopp (ref. 2), who devised a method to correct for it. Subsequently, Mangler and Spencer (ref. 19) introduced a better method and Garner (ref. 20) illustrated the importance of this correction. This method of correcting for the logarithmic singularity has been

used for the flap pressure mode and is reproduced here. Only the most important terms are retained (i.e., $(\partial h/\partial x')(x, \eta')$ and $c(\eta')$ are replaced by $(\partial h/\partial x)(x, \eta)$ and $c(\eta)$). The proper edge behavior must be introduced into the singular part; accordingly, it is multiplied by the factor $\sqrt{1-\eta'^2}/\sqrt{1-\eta^2}$. The singularity is then added and subtracted from the integrand, giving the following expression for the flap downwash mode:

$$\alpha_f(\xi, \eta) = \frac{\cos \lambda_c}{4\pi^2 \sqrt{1-M^2} \cos^2 \lambda_c} \left\{ \int_{-1}^{+1} \left[\frac{C_2(\eta') \frac{c(\eta')}{b}}{(\eta' - \eta)^2} H_f(\xi, \eta, \eta') \right. \right. \\ \left. \left. + C_2(\eta) \beta^2 \frac{b}{c(\eta)} \frac{\partial h}{\partial x'}(x, \eta) \frac{\sqrt{1-\eta'^2}}{\sqrt{1-\eta^2}} \ln |\eta - \eta'| \right] d\eta' \right. \\ \left. - \frac{C_2(\eta) \beta^2 b}{\sqrt{1-\eta^2} c(\eta)} \frac{\partial h}{\partial x'}(x, \eta) \int_{-1}^{+1} \sqrt{1-\eta'^2} \ln |\eta - \eta'| d\eta' \right\} \quad (B3)$$

The bracketed term will not contain a logarithmic singularity and is integrated numerically by Multhopp's integration formula. The integral in the last term has been done analytically in reference 20:

$$\int_{-1}^{+1} \sqrt{1-\eta'^2} \ln |\eta' - \eta| d\eta' = \frac{\pi}{4} [2\eta^2 - 1 - \ln 4] \quad (B4)$$

The expression for $h(x', \eta')$ is

$$h(x', \eta') = \sqrt{\frac{1-x'^2}{1-x_c^2}} \ln \left[\frac{\sqrt{(x' - x_c)^2 + y_1^2} - y_1}{\sqrt{(x' - x_c)^2 + y_2^2} - y_2} \right] \quad (B5)$$

which, when combined with equations (B3) and (B4), will yield the final form of the equation for the flap mode of pressure for an interior control point. For a control point on a wing leading edge ($x' = -1$) or trailing edge ($x' = +1$), however, $\partial h/\partial x'$ becomes infinite, violating the assumption that $h(x', \eta')$ can be developed in a Taylor series.

The appropriate approach in either instance is to retain the square-root behavior in the chordwise integral and to develop the remainder of the function $h(x', \eta')$ in a Taylor series about the leading- or trailing-edge point. This approach was used by Jordan (ref. 21) for regular pressure modes. When applied to the flap pressure modes, the following expression has been derived for the lowest order irregular term in the flap influence function for the leading edge:

$$\Delta H_f(\xi, \eta, \eta') = \frac{16}{3\sqrt{1-x_c^2}} \ln \left| \frac{\sqrt{(1+x_c)^2 + y_1^2} - y_1}{\sqrt{(1+x_c)^2 + y_2^2} - y_2} \right| \cdot \left| \frac{b\beta}{2c(\eta) \cos \phi_{\lambda e}} \right|^{3/2} F_1(m_{\lambda e}) |\eta' - \eta|^{3/2} \quad (B6a)$$

where $F_1(m_{\ell e}) = (2m_{\ell e} - 1)E(m_{\ell e}) + (1 - m_{\ell e})K(m_{\ell e})$ (B6b)

$$m_{\ell e} = \frac{1}{2} (1 + \sin \phi_{\ell e}) \quad (B6c)$$

$$\phi_{\ell e} = \tan^{-1} \left[\frac{1}{\beta} \tan \lambda_{\ell e} \right] \quad (B6d)$$

where $\lambda_{\ell e}$ is the leading-edge sweep angle at the control point defined so that $-\pi/2 < \lambda_{\ell e} < +\pi/2$ and $\lambda_{\ell e} > 0$ on that side of the control point for which the edge sweeps forward. The leading-edge sweep angle is of the opposite sign on the other side (assuming no kink in the leading edge). The corresponding formula for the trailing edge is

$$\Delta H_f(\xi, \eta, \eta') = - \frac{16}{3\sqrt{1-x_c^2}} \ln \left| \frac{\sqrt{(1-x_c)^2 + y_1^2} - y_1}{\sqrt{(1-x_c)^2 + y_2^2} - y_2} \right| \cdot \left| \frac{b\beta}{2c(\eta) \cos \phi_{te}} \right|^{3/2} F_1(m_{te}) |\eta' - \eta|^{3/2} \quad (B7a)$$

where

$$m_{te} = \frac{1}{2} (1 - \sin \phi_{te}) \quad (B7b)$$

$$\phi_{te} = \tan^{-1} \left[\frac{1}{\beta} \tan \lambda_{te} \right] \quad (B7c)$$

The term λ_{te} is defined as for the leading edge. Note that in either case the parameter, m , of the elliptic integrals changes on passing from one side of the control point to the other (more precisely, if m^+ is the value for $\eta' > \eta$, then $1 - m^+$ is the value for $\eta' < \eta$ if there is no kink at $\eta' = \eta$). As in the case of interior points, this irregularity is, after introducing the factor $\sqrt{1-\eta'^2}/\sqrt{1-\eta^2}$ to account for the edge behavior, simultaneously added and subtracted from the integrand, leaving a part to integrate analytically and a smoother part to integrate numerically. At the leading edge, equation (B6a) is actually the leading term, so the spanwise integral does not have the second-order pole, but rather one of order $-1/2$. After this is eliminated by adding and subtracting the irregular part (eq. (B6a)), the leading term of the integrand in the vicinity of $\eta' = \eta$ would be a constant followed by terms of order $1/2, 1, \text{etc.}$ Multhopp's integration formula may still be conveniently used for this integration. The integral for the leading edge is thus

$$\alpha_f(\xi, \eta) = \frac{\cos \lambda_c}{4\pi^2 \sqrt{1-M^2} \cos^2 \lambda_c} \left\{ \int_{-1}^{+1} \left[\frac{C_2(\eta') \frac{c(\eta')}{b}}{(\eta' - \eta)^2} H_f(\xi, \eta, \eta') \right. \right. \\ \left. \left. - \frac{\sqrt{1-\eta'^2}}{\sqrt{1-\eta^2}} C_2(\eta) \frac{c(\eta)}{b} \frac{16}{3\sqrt{1-x_c^2}} \ln \left| \frac{\sqrt{(1+x_c)^2 + y_1^2} - y_1}{\sqrt{(1+x_c)^2 + y_2^2} - y_2} \right| \right. \right.$$

(equation continued on the following page)

$$\begin{aligned}
& \times \left(\frac{b\beta}{2c(\eta)\cos\phi_{\ell e}} \right)^{3/2} F_1(m_{\ell e}) |n'-\eta|^{-1/2} \Big] d\eta' + \int_{-1}^{+1} \sqrt{\frac{1-\eta'^2}{1-\eta^2}} C_2(\eta) \frac{c(\eta)}{b} \frac{16}{3\sqrt{1-x_c^2(\eta)}} \\
& \times \ln \left| \frac{\sqrt{(1+x_c)^2+y_1^2} - y_1}{\sqrt{(1+x_c)^2+y_2^2} - y_2} \right| \left(\frac{b\beta}{2c(\eta)} \right)^{3/2} \frac{F_1(m_{\ell e})}{(\cos\phi_{\ell e})^{3/2}} |n'-\eta|^{-1/2} d\eta' \Big\}
\end{aligned} \tag{B8}$$

The bracketed term is not singular and is computed using Multhopp's formula. The last term, computed analytically, is also expressed in terms of elliptic integrals:

$$\begin{aligned}
& \int_{-1}^{+1} \frac{\sqrt{1-\eta'^2}}{(\cos\phi_{\ell e})^{3/2}} \frac{F_1(m_{\ell e})}{|n'-\eta|^{-1/2}} d\eta' \\
& = \frac{2\sqrt{2}}{3(\cos\phi_{\ell e})^{3/2}} \left\{ F_1(m_{\ell e}^-) [(1-\eta)K(m) + 2\eta E(m)] + F_1(m_{\ell e}^+) [(1+\eta)K(1-m) - 2\eta E(1-m)] \right\}
\end{aligned} \tag{B9a}$$

where $m = \frac{1+\eta}{2}$ (B9b)

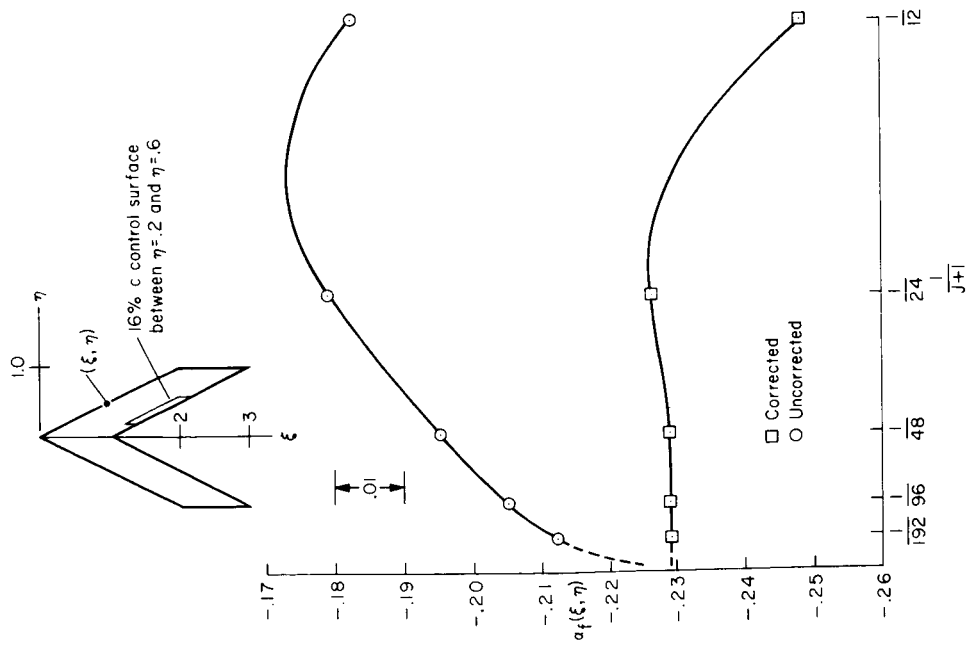
Therefore, for the leading edge,

$$\begin{aligned}
\alpha_f(\xi, \eta) & = \frac{\cos\lambda_c}{4\pi^2\sqrt{1-M^2}\cos^2\lambda_c} \left(\int_{-1}^{+1} \left[\frac{C_2(\eta') \frac{c(\eta')}{b}}{(n'-\eta)^2} H_f(\xi, \eta, \eta') \right. \right. \\
& - \frac{\sqrt{1-\eta'^2}}{\sqrt{1-\eta^2}} C_2(\eta) \frac{c(\eta)}{b} \frac{16}{3\sqrt{1-x_c^2}} \ln \left| \frac{\sqrt{(1+x_c)^2+y_1^2} - y_1}{\sqrt{(1+x_c)^2+y_2^2} - y_2} \right| \\
& \times \left. \left(\frac{b\beta}{2c(\eta)\cos\phi_{\ell e}} \right)^{3/2} F_1(m_{\ell e}) |n'-\eta|^{-1/2} \right] d\eta' \\
& + \frac{C_2(\eta)}{\sqrt{1-\eta^2}} \frac{c(\eta)}{b} \frac{16}{3\sqrt{1-x_c^2(\eta)}} \ln \left| \frac{\sqrt{(1+x_c)^2+y_1^2} - y_1}{\sqrt{(1+x_c)^2+y_2^2} - y_2} \right| \left(\frac{b\beta}{2c(\eta)\cos\phi_{\ell e}} \right)^{3/2} \\
& \cdot \frac{2\sqrt{2}}{3} \{ F_1(m_{\ell e}^-) [(1-\eta)K(m) + 2\eta E(m)] + F_1(m_{\ell e}^+) [(1+\eta)K(1-m) - 2\eta E(1-m)] \}
\end{aligned} \tag{B10}$$

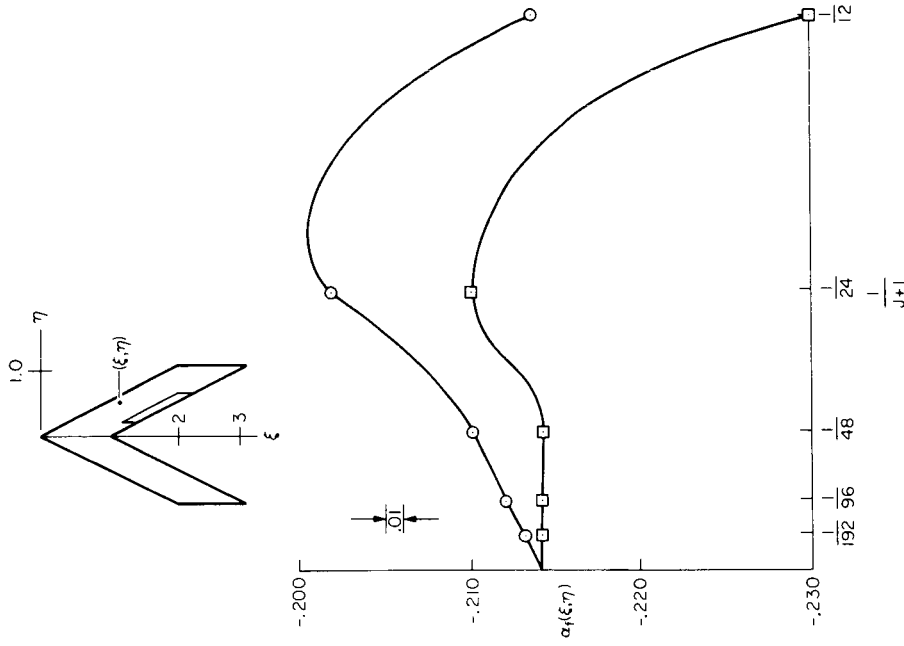
For the trailing edge,

$$\begin{aligned}
 \alpha_f(\xi, \eta) = & \frac{\cos \lambda_c}{4\pi^2 \sqrt{1-M^2} \cos^2 \lambda_c} \left(\int_{-1}^{+1} \left[\frac{C_2(\eta') \frac{c(\eta')}{b}}{(\eta' - \eta)^2} H_f(\xi, \eta, \eta') \right. \right. \\
 & + \frac{\sqrt{1-\eta'^2}}{\sqrt{1-\eta^2}} C_2(\eta) \frac{c(\eta)}{b} \frac{16}{3\sqrt{1-x_c^2}} \ln \left| \frac{\sqrt{(1-x_c)^2 + y_1^2} - y_1}{\sqrt{(1-x_c)^2 + y_2^2} - y_2} \right| \\
 & \times \left. \left. \left(\frac{b\beta}{2c(\eta) \cos \phi_{te}} \right)^{3/2} F_1(m_{te}^-) | \eta' - \eta |^{-1/2} \right] d\eta' \right. \\
 & - \frac{C_2(\eta)}{\sqrt{1-\eta^2}} \frac{c(\eta)}{b} \frac{16}{3\sqrt{1-x_c^2}} \ln \left| \frac{\sqrt{(1-x_c)^2 + y_1^2} - y_1}{\sqrt{(1-x_c)^2 + y_2^2} - y_2} \right| \left(\frac{b\beta}{2c(\eta) \cos \phi_{te}} \right)^{3/2} \\
 & \left. \left. \cdot \frac{2\sqrt{2}}{3} [F_1(m_{te}^-) [(1-\eta)K(m) + 2\eta E(m)] + F_1(m_{te}^+) [(1+\eta)K(1-m) - 2\eta E(1-\eta)]] \right) \right)
 \end{aligned}
 \tag{B11}$$

It is important to note that values for x_c , y_1 , y_2 , ϕ_{le} , and ϕ_{te} appearing in the above equations are to be evaluated at the control point, η . An appropriate question might be: "How important are these corrections?" The answer is supplied by figures 17(a) through (e), which show downwash values calculated for various points on a sample wing for various numbers of spanwise integration points, J . These graphs clearly show that it is important to use these corrections, at least when Multhopp's integration formula is used. For other integration procedures (i.e., the zonal scheme of Watkins et al. (ref. 22)), this method of correction could also be applied. Although it is not known how important the corrections would be, it seems, in view of how well they worked for Multhopp's method, that they could be significantly worthwhile. Figure 17 also shows how close $\alpha_f(\xi, \eta)$ can be predicted. An appropriate number to compare these values with is 1, since the flap pressure mode produces a discontinuity of magnitude 1. For $J = 191$, the error is less than 0.3 percent for all points, except for the one which is only 1.4 percent c behind the hinge line. The error for this point is approximately 6 percent. When computing $\alpha_f(\xi, \eta)$ for the lifting surface program, however, N can be chosen so that all or most of the collocation points are not so near the hinge line. The spanwise control point positions are chosen so that they are not near the side edges of the control surface.



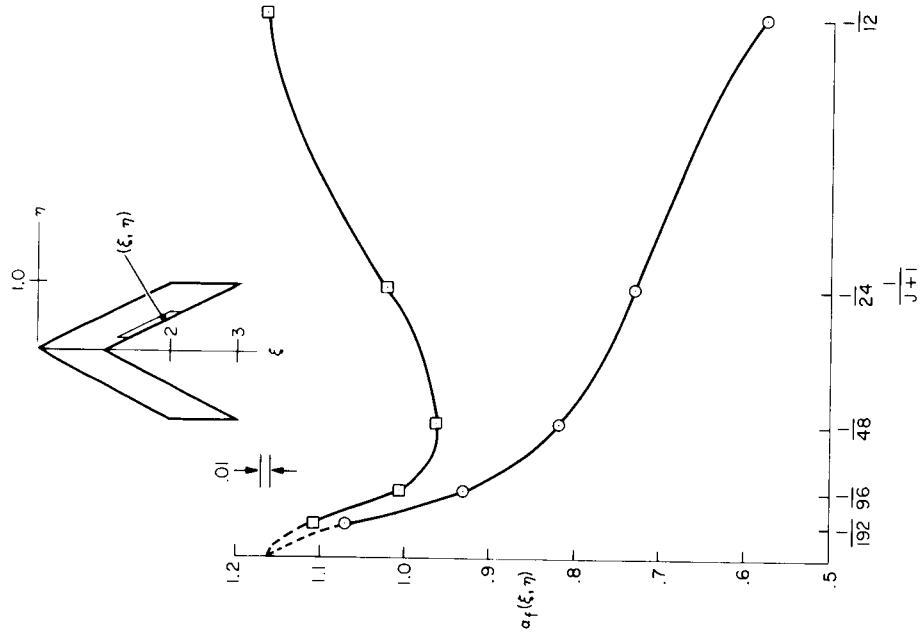
(a) At the leading edge and 50% semispan station.



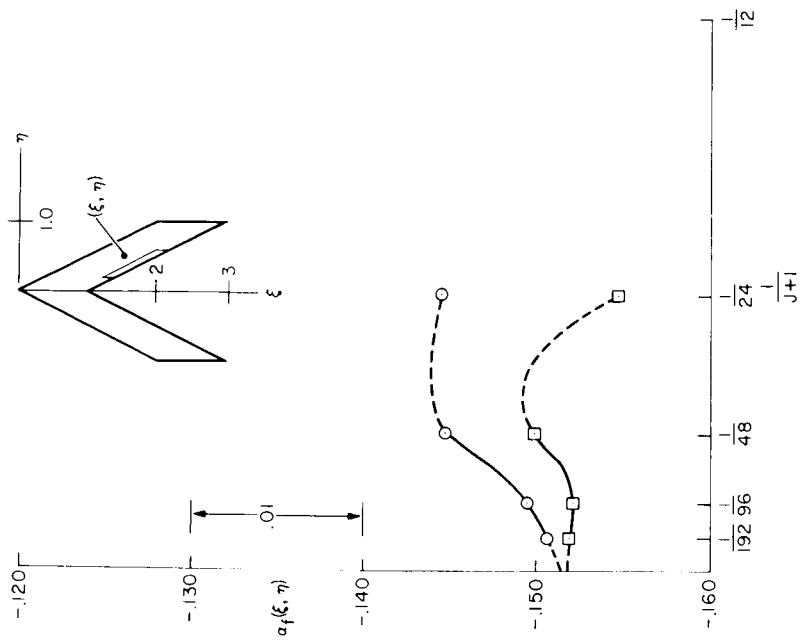
(b) At the 14.64% chord and 50% semispan station.

Figure 17.- Effect of using the spanwise correction formulas for computing the flap downwash mode for various numbers of spanwise integration points, J .

Figure 17.- Continued.

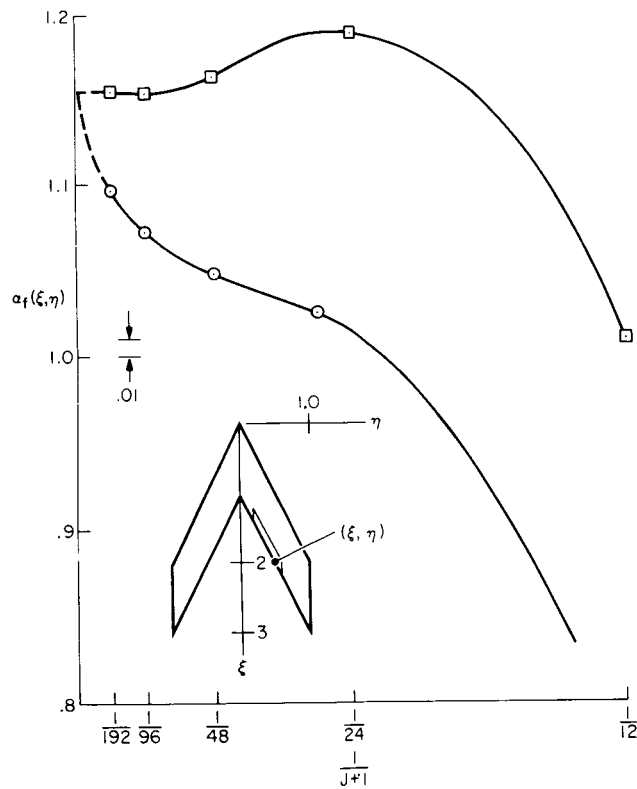


(d) At the 85.36% chord and 50% spanwise station.



(c) At the 50% chord and 50% semispan station.

Figure 17.- Concluded.



(e) At the trailing edge and 50% semispan station.

REFERENCES

1. Landahl, M.: Pressure-Loading Functions for Oscillating Wings With Control Surfaces. AIAA J., vol. 6, no. 2, Feb. 1968, pp. 345-348.
2. Multhopp, Hans: Methods for Calculating the Lift Distribution of Wings (Subsonic Lifting-Surface Theory). R. & M. 2884, British A.R.C., Jan. 1950.
3. Truckenbrodt, E.: Tragflächentheorie bei Inkompressibler Strömung. Wissenschaftliche Gesellschaft für Luftfahrt, Jahrbuch 1953, pp. 40-65.
4. Hsu, Pao-Tan; and Weatherill, Warren H.: Pressure Distribution and Flutter Analysis of Low-Aspect-Ratio Wings in Subsonic Flow. ASRL Tech. Rept. 64-3, Massachusetts Inst. Technol., June 1959.
5. Ashley, Holt and Landahl, Marten T.: Aerodynamics of Wings and Bodies. Addison-Wesley, Reading, Mass., 1965.
6. Wagner, Siegfried: On the Singularity Method of Subsonic Lifting Surface Theory. AIAA Paper 69-37, 1969; also J. Aircraft, vol. 6, no. 6, Nov.-Dec., 1969, pp. 549-558.
7. Kussner, H. G.; and Schwarz, L.: Luftfahrtforschung 17, 1940, pp. 337-354 (Transl.: The Oscillating Wing with Aerodynamically Balanced Elevator. NACA TM 991, 1941).
8. Hildebrand, Francis B.: A Least-Squares Procedure for the Solution of the Lifting-Line Integral Equation. NACA TN 925, 1944.
9. Crespo, A. N.; and Cunningham, H. J.: Development of Three-Dimensional Pressure-Distribution Functions for Lifting Surfaces with Trailing-Edge Controls Based on the Integral Equation for Subsonic Flow. NASA TN D-5419, 1969.
10. Rowe, W. S.: Collocation Method for Calculating the Aerodynamic Pressure Distributions on a Lifting Surface Oscillating in Subsonic Compressible Flow. Proc. AIAA Symposium on Structural Dynamics and Aeroelasticity, Boston, 1965, pp. 31-45.
11. Zandbergen, P. J.; Labrujere, Th. E.; and Wouters, J. G.: A New Approach to the Numerical Solution of the Equation of Subsonic Lifting Surface Theory. National Aerospace Lab. Rept. NLR-TR-G-49, The Netherlands, Nov. 1967.
12. Hammond, Alexander D.; and Keffer, Barbara M.: The Effect at High Subsonic Speeds of a Flap-Type Aileron on the Chordwise Pressure Distribution Near Midsemispan of a Tapered 35° Sweptback Wing of Aspect Ratio 4 Having NACA 65A006 Airfoil Section. NACA RM L53C23, 1953.

13. Garner, H. C.; and Miller, G. F.: Analytical and Numerical Studies of Downwash Over Rectangular Planforms. National Physical Lab. (UK) Rept. NPL-MA-99, May 1971.
14. Carmichael, Ralph L.; Castellano, Charles R.; and Chen, Chuan F.: The Use of Finite Element Methods for Predicting the Aerodynamics of Wing-Body Combinations. NASA SP-228, 1970, pp. 37-51.
15. Giesing, J. P.: Lifting Surface Theory for Wing-Fuselage Combinations. Rept. DAC-67212, vol. 1, McDonnell Douglas Aircraft Co., Aug. 1968.
16. Fink, Marvin P.; and Cocke, Bennie W.: A Low-Speed Investigation of the Aerodynamic, Control- and Hinge-Moment Characteristics of Two Types of Controls and Balancing Tabs on a Large-Scale Thin Delta-Wing Fuselage Model. NACA RM L54B03, 1954.
17. Pfyl, Frank A.: Aerodynamic Study of a Wing-Fuselage Combination Employing a Wing Swept Back 63° - Effectiveness of an Inboard Elevon as a Longitudinal- and Lateral-Control Device at Subsonic and Supersonic Speeds. NACA RM A51118, 1951.
18. Ashley, H.: Subsonic Oscillatory or Steady Airloads on Wings With Control Surfaces and Other Discontinuities. SUDAAR Rept. 336, Stanford Univ., Dec. 1967.
19. Mangler, K. W.; and Spencer, B. F. R.: Some Remarks on Multhopp's Lifting Surface Theory. R. & M. No. 2926, British A.R.C., Aug. 1952.
20. Garner, H. C.: Accuracy of Downwash Evaluation by Multhopp's Lifting-Surface Theory. R. & M. No. 3431, British A.R.C., 1966.
21. Jordan, P. F.: Wing-Edge Pivot Points in Subsonic Lifting Surface Analysis. RIAS-TR-69-17C, Martin Marietta Corp., Baltimore, Maryland, Nov. 1969.
22. Watkins, Charles E.; Woolston, Donald S.; and Cunningham, Herbert J.: A Systematic Kernel Function Procedure for Determining Aerodynamic Forces on Oscillating or Steady Finite Wings at Subsonic Speeds. NASA TR R-48, 1959.